Astron. Astrophys. 356, 1039–1049 (2000)

ASTRONOMY AND ASTROPHYSICS

Deuterium fractionation in dense ammonia cores

S. Tiné[1], E. Roueff[2], E. Falgarone[3], M. Gerin[4], and G. Pineau des Forêts[5]

[1] Observatoire de Paris-Meudon, 92195 Meudon, France (Stefano.Tine@obspm.fr)
[2] Observatoire de Paris-Meudon, 92195 Meudon, France (Evelyne.Roueff@obspm.fr)
[3] Ecole Normale Supérieure, 75231 Paris, France (Edith.Falgarone@lra.ens.fr)
[4] Ecole Normale Supérieure, 75231 Paris, France (Maryvonne.Gerin@lra.ens.fr)
[5] Observatoire de Paris-Meudon, 92195 Meudon, France (Guillaume.PineauDesForets@obspm.fr)

Received 24 December 1999 / Accepted 18 February 2000

Abstract. We report observations of several deuterated species in the dark clouds L134N and TMC1, and in particular of NH_2D (deuterated ammonia). NH_2D has been detected for the first time towards the dense core TMC1-N and very strong emission has been confirmed towards L134N. The deuterium fractionation is very different in these two clouds, with abundance ratio $[NH_2D]/[NH_3] \sim 0.1$ and ~ 0.02, $[N_2D^+]/[N_2H^+] \sim 0.35$ and ~ 0.08 and $[DCO^+]/[HCO^+] \sim 0.18$ and ~ 0.02, towards L134N and TMC1-N, respectively. For both clouds, but most clearly for L134N, the region of high deuterium fractionation is more localized and much more compact than the high column density region traced by $C^{18}O$ and $C^{17}O$ emission. We compare the observed deuterium fractionation with steady-state chemical models and we find that a better match is obtained when C and O are heavily depleted from the gas phase.

Key words: ISM: individual objects: L134N – ISM: individual objects: TMC1 – ISM: molecules

1. Introduction

Observationally, ammonia is largely used as a tracer of dense cores (Myers & Benson 1983) as it is found in high extinction regions, and shows narrow lines with little contribution from turbulence. As it belongs to the class of molecules formed late in the chemical evolution of dark clouds, ammonia is expected to be found in the quietest and densest parts of such objects. Indeed, this seems to be the case for the dense core L1498 (Kuiper et al. 1996). In this core, NH_3 is found to be the most centrally condensed molecule, whereas CS is found in a shell just exterior to the ammonia core and $C^{18}O$ lines trace an even more extended envelope.

Similarly, deuterated species are expected to be found in the coldest regions of dark clouds, where gas phase ion-molecule chemistry is at work. Deuterium fractionation starts with exothermic exchange reactions of molecular ions (H_3^+, CH_3^+, etc.) with HD, while inverse reactions are inhibited by the resulting endothermicity which is of the order of some hundred Kelvins. Therefore, a high degree of deuteration can occur and abundance ratios of deuterated/normal species ranging from 2 to 10% can be predicted, in good agreement with the reported figures (Penzias et al. 1977; Snell & Wootten 1977; Brown & Rice 1981; Wootten et al. 1982; Guélin et al. 1982, Snyder et al. 1977).

For these reasons combined, deuterated ammonia is expected to be abundant in dense cores. After the first unambiguous detection in such regions by Olberg et al. (1985), who found NH_2D towards L183 (which is $\sim 1'$ SE of the reference position for L134N adopted here), Saito et al. (2000) detected NH_2D in a number of dark molecular clouds including L134N, whereas their search towards TMC1 was unsuccessful.

In the present paper, we report the first detection of deuterated ammonia towards TMC1 and present the first maps of NH_2D towards L134N and TMC1-N. We also compare these maps of NH_2D with other tracers of dark clouds: $C^{18}O$, for the total column density, and DCO^+, as an example of another deuterated molecule. Towards selected lines of sight, we also derive column densities for $C^{17}O$, $H^{13}CO^+$ and for another two nitrogen carrying molecules, N_2D^+ and N_2H^+, in order to constrain further the physical conditions and deuterium enrichment of the gas. We first describe the observations (Sect. 2), then present the results (Sect. 3) and finally discuss them in the light of gas phase chemical models (Sect. 4).

2. Observations

The observations have been performed with the 30m IRAM telescope in Pico Veleta (Spain) between July 1997 and January 1999. The weather conditions were averaged in summers (T_{sys} = 250K at 110 GHz), where single positions only have been observed. We had very good weather in January 1999 (T_{sys} = 150K) and performed maps around the strongest position, with a spacing of $20''$ on both axes. The telescope is equipped with SIS receivers operated in single side band (SSB). The observations were performed in frequency switching mode (FS) with the frequency throw set to 7.7 MHz for the 3mm lines (and appropriate scaling for the higher frequencies), large enough to

Send offprint requests to: E. Roueff
Correspondence to: DAEC, Observatoire de Paris-Meudon, 5 Place Janssen, 92195 Meudon, France

avoid blending of the hyperfine components. As a backend, we used the autocorrelator with a very high frequency resolution: 20 kHz for the 2mm and 3mm lines and 40 kHz for the 1mm lines. The corresponding velocity resolution is $\simeq 0.05$ kms^{-1}. The only exception is for the $C^{18}O$ mapping where we used a backend with 100 kHz resolution, corresponding to a velocity resolution of 0.3 kms^{-1}. The half power beam width (HPBW) of the 30m telescope is 22″ at 110 GHz, and 11″ at 230 GHz. At these frequencies the main beam efficiency is approximately 0.66 and 0.42, respectively.

In October 1999, we performed additional observations of the pure rotational transitions connecting the ground and first excited states of NH_2D with the Caltech Submillimeter Observatory (CSO). These transitions lie around 332 GHz and the observations have been performed in position switching mode, using two acousto-optic spectrometers (AOS) as backends, with a frequency resolution of 100 kHz and 1 MHz respectively. The HPBW of the CSO is 21″, and the main beam efficiency is 0.65.

The spectroscopic parameters of the observed lines are reported in Table 1, which lists for each observed transition the rest frequency, upper level energy, Einstein coefficient and, in case of hyperfine splitting, the relative intensity of each component. The values reported for NH_2D have been calculated by Coudert (1999). The program has been checked with the Stark C_2 coefficients values (Roueff et al. 2000) and comparing them with the observed values given by Cohen & Pickett (1982).

We mapped two regions: the first one near the reference position of the L134N dark cloud (RA(1950) = $15^h51^m30^s.0$, Dec (1950) = -02*d*o43′31″) and the second one close to the ammonia peak in TMC1 (RA(1950) = $4^h38^m17.3^s$, Dec (1950) = 25°42′23.2″, hereafter TMC1-N). These two positions were selected as N_2H^+ peaks on maps made with the 14m FCRAO antenna (Pratap et al. 1997; Irvine 1998).

3. Results

3.1. Detection and morphology

The lines were fitted with Gaussian profiles. In Table 2, we report the peak temperature, integrated intensity, noise level, central velocity and line width for each line, in the T_A^* scale. The accuracy of the figures depends on the signal to noise ratio, and also on the overall accuracy of the calibration which is about 25%.

3.1.1. NH_2D

We detected NH_2D in L134N and TMC1-N in the two rotation-inversion ladders connecting the $1_{1,1}$-$1_{0,1}$ levels around 85.9 and 110.1 GHz respectively. The hyperfine structure is well resolved. The two patterns correspond to the ortho and para forms of NH_2D (Olberg et al. 1985). The corresponding nuclear statistical weights are 3 and 1. Individual spectra for L134N at offset (30″,18″) and for TMC1-N are shown in Fig. 1 for both lines. The pattern at 85 GHz corresponding to ortho states is more prominent due to the larger statistical weight. These transitions are associated with the largest dipole moment for this

Table 1. Spectroscopic parameters of the observed lines

Transition	Frequency (MHz)	E_u (K)	A (s^{-1})	I/I_t
$C^{18}O$				
J=1-0	109782.1734	5.3	6.3(-8)	1.000
J=2-1	219560.3568	15.8	6.0(-7)	1.000
$C^{17}O$				
J=2-1 F=3/2-5/2	224713.5011	16.2	1.9(-7)	0.040
J=2-1 F=5/2-5/2	224714.0451	16.2	3.9(-7)	0.122
J=2-1 F=7/2-5/2	224714.1551	16.2	4.1(-7)	0.171
J=2-1 F=9/2-7/2	224714.1998	16.2	6.4(-7)	0.333
J=2-1 F=1/2-3/2	224714.2141	16.2	6.5(-7)	0.067
J=2-1 F=3/2-3/2	224714.7261	16.2	4.5(-7)	0.093
J=2-1 F=5/2-7/2	224715.0627	16.2	5.1(-8)	0.016
J=2-1 F=7/2-7/2	224715.1728	16.2	2.3(-7)	0.095
J=2-1 F=5/2-3/2	224715.2701	16.2	2.0(-7)	0.062
$H^{13}CO^+$				
J=1-0	86754.3300	4.2	2.8(-5)	1.000
DCO^+				
J=2-1	144077.3190	10.4	1.5(-4)	1.000
J=3-2	216112.6045	20.7	5.5(-4)	1.000
NH_2D				
(ortho)				
$1_{1,1}$-$1_{0,1}$ F=0-1	85924.7829	20.7	7.8(-6)	0.111
$1_{1,1}$-$1_{0,1}$ F=2-1	85925.7031	20.7	2.0(-6)	0.139
$1_{1,1}$-$1_{0,1}$ F=2-2	85926.2703	20.7	5.9(-6)	0.417
$1_{1,1}$-$1_{0,1}$ F=1-1	85926.3165	20.7	2.0(-6)	0.083
$1_{1,1}$-$1_{0,1}$ F=1-2	85926.8837	20.7	3.3(-6)	0.139
$1_{1,1}$-$1_{0,1}$ F=1-0	85927.7345	20.7	2.6(-6)	0.111
–				
$1_{0,1}$-$0_{0,0}$ F=0-1	332780.9447	16.5	7.8(-6)	0.111
$1_{0,1}$-$0_{0,0}$ F=2-1	332781.7955	16.5	7.8(-6)	0.556
$1_{0,1}$-$0_{0,0}$ F=1-1	332782.3627	16.5	7.8(-6)	0.333
–				
(para)				
$1_{1,1}$-$1_{0,1}$ F=0-1	110152.0963	21.3	1.7(-5)	0.111
$1_{1,1}$-$1_{0,1}$ F=2-1	110153.0165	21.3	4.1(-6)	0.139
$1_{1,1}$-$1_{0,1}$ F=2-2	110153.5868	21.3	1.2(-5)	0.417
$1_{1,1}$-$1_{0,1}$ F=1-1	110153.6299	21.3	4.1(-6)	0.083
$1_{1,1}$-$1_{0,1}$ F=1-2	110154.2002	21.3	6.9(-6)	0.139
$1_{1,1}$-$1_{0,1}$ F=1-0	110155.0557	21.3	5.5(-6)	0.111
–				
$1_{0,1}$-$0_{0,0}$ F=0-1	332821.5595	15.9	7.3(-6)	0.111
$1_{0,1}$-$0_{0,0}$ F=2-1	332822.4149	15.9	7.3(-6)	0.556
$1_{0,1}$-$0_{0,0}$ F=1-1	332822.9853	15.9	7.3(-6)	0.333
N_2H^+				
J=1-0 F_1=1-1 F=0-1	93171.6500	4.5	3.4(-5)	0.037
J=1-0 F_1=1-1 F=2-2	93171.9400	4.5	3.4(-5)	0.185
J=1-0 F_1=1-1 F=1-1	93172.0800	4.5	3.4(-5)	0.111
J=1-0 F_1=2-1 F=2-1	93173.5050	4.5	3.4(-5)	0.185
J=1-0 F_1=2-1 F=3-2	93173.8000	4.5	3.4(-5)	0.259
J=1-0 F_1=2-1 F=1-0	93174.0000	4.5	3.4(-5)	0.111
J=1-0 F_1=0-1 F=1-2	93176.2900	4.5	3.4(-5)	0.111
N_2D^+				
J=2-1	154217.0960	11.1	2.0(-4)	1.000
J=3-2	231321.6650	22.2	7.1(-4)	1.000

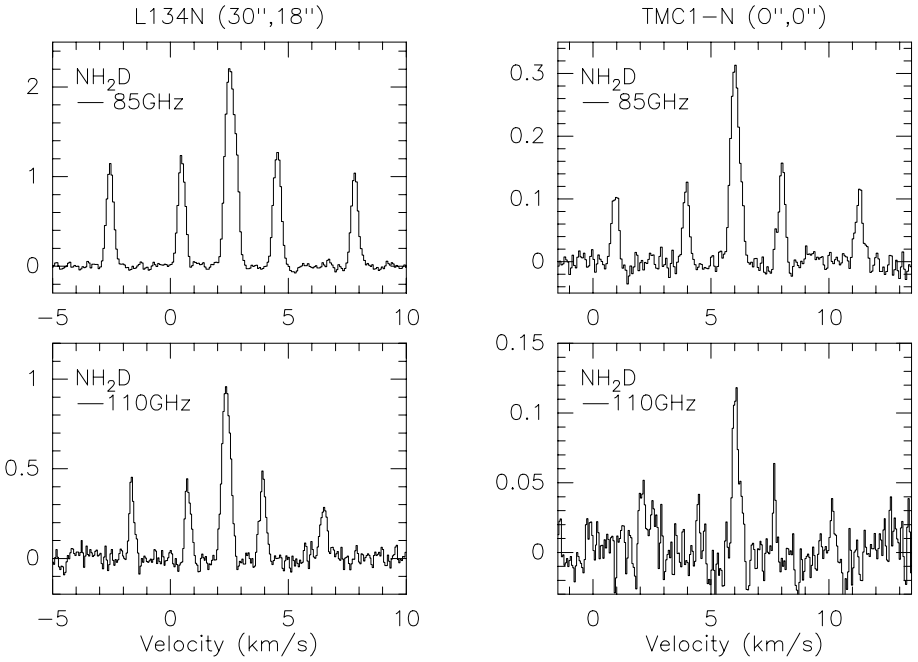

Fig. 1. NH_2D spectra obtained at the IRAM 30m telescope. The temperature unit is T_A^* in Kelvins, velocities are calculated in the LSR. Left column is for L134N (30″,18″), right column is for TMC1-N (0″,0″). The velocity range (x-axis) is the same for all four spectra, but note the change of scale on the y-axis between left and right columns.

molecule (μ_c=1.463 Debye) and the blend with a transition of methyl formate ($HCOOCH_3$), which hampers conclusive detection of these lines in hotter regions (Cummins et al. 1986; Jacq et al. 1990), is irrelevant in the present context of dark quiescent clouds. We also detected, at the 3–4σ level, the weaker pure rotational transitions at 332.78 GHz (ortho) and 332.82 GHz (para), which are associated with a smaller dipole moment (μ_a=-0.18 Debye).

To our knowledge, the detection of NH_2D towards TMC1-N is the first one.

For both clouds, the rotation-inversion lines are extremely narrow (Δv$\simeq$0.35 km s^{-1}), narrower than the DCO^+ lines, but similar to the NH_3 line width. For NH_2D, the thermal line width (FWHM) corresponding to a kinetic temperature of 10 K is 0.16 km s^{-1} while the thermal line width for H_2 is 0.48 km s^{-1}. Turbulent motions contribute therefore to a large extent to the observed line width, as is the case for NH_3.

We show in Figs. 2a and 3a maps of the 110 GHz transitions of NH_2D towards L134N and TMC1-N, respectively. It can be seen that intense NH_2D emission is confined to a small region. The extent of the NH_2D emission is about 1′ or 0.04 pc at the distance of the clouds (140 pc).

3.1.2. Other molecules

We have also observed N_2H^+(1-0) and N_2D^+(2-1) towards both dense cores. The N_2H^+(1-0) spectra are shown in Fig. 4 where the hyperfine structure due to both nitrogen nuclei is well resolved.

In Fig. 5, we show spectra of two isotopic substitutes of CO, i.e. $C^{17}O$ and $C^{18}O$, as well as $H^{13}CO^+$, DCO^+ and N_2D^+ lines. While N_2H^+ and N_2D^+ show narrow lines (Δv$\simeq$0.30–0.40 kms^{-1}), the $H^{13}CO^+$ and DCO^+ are somewhat broader and flat topped, and those of $C^{17}O$ and $C^{18}O$ reach 0.6 kms^{-1}.

In Figs. 2 and 3 we also show maps of other selected lines towards L134N and TMC1-N, for comparison with the maps of NH_2D discussed above. Note how the $C^{18}O$ emission shows little variation in the map, in contrast with NH_2D. The DCO^+ map shows a peak, but this molecule appears to be less confined to a small region than is NH_2D. Towards L134N we were also able to map N_2D^+(2-1), and in this case the emission mimics well the distribution of deuterated ammonia.

3.2. Column densities and physical conditions

We limit the discussion of column densities and physical conditions (and chemical models, see next section) to one position in each cloud: offset (30”,18”) of L134N and the reference position (0,0) in TMC1-N. Both positions were chosen as representative of the peak emission of deuterated species.

We used the main beam temperature scale for all spectra to derive column densities. For the lines with hyperfine structure we adopted where possible the HFS method of CLASS, part of the GILDAS software package which returns the total optical depth τ and average line width of the lines in an LTE approximation as well as the radiation temperature of the multiplet, T_R. From these quantities the excitation temperature T_{ex} for the multiplet, can be derived from the following equation

$$T_R = [J_\nu(T_{ex}) - J_\nu(T_{bg})](1 - e^{-\tau}) \quad (1)$$

where $J_\nu(T)$ is the radiation temperature of a black body at temperature T and T_{bg}=2.7 K (the temperature of the cosmic background radiation).

From the optical depth, excitation temperature and average FWHM Δv, we deduce the total column density for the molecule as follows

$$N = \frac{8\pi\nu_{ul}^3}{c^3}\frac{Q(T_{ex})}{g_u A_{ul}}\Delta v \frac{e^{\frac{E_u}{kT_{ex}}}}{e^{\frac{h\nu}{kT_{ex}}} - 1}\tau_{ul} \quad (2)$$

Table 2. Results of Gaussian fits to lines

Molecule	Line	T_A^* (K)	$\int T_A^* dv$ (Kkms^{-1})	σ (K)	v_{LSR} (kms^{-1})	Δv (kms^{-1})
L134N (30″,18″)						
$C^{18}O$	J=1-0	2.84	1.30	0.08	2.5	0.43
	J=2-1	2.22	1.21	0.06	2.5	0.51
$C^{17}O$	J=2-1	0.53[a]	0.25[b]	0.05	2.8	0.38
$H^{13}CO^+$	J=1-0	0.84	0.45	0.07	2.5	0.51
DCO^+	J=2-1[c]	1.49	0.93	0.12	2.3	0.59
	J=3-2	1.09	0.54	0.06	2.5	0.47
NH_2D (ortho)	85 GHz	2.25[a]	3.06[b]	0.03	2.6	0.37
	332 GHz	0.40[a]	0.30[b]	0.07	2.3	-
NH_2D (para)	110 GHz	0.98[a]	0.93[b]	0.04	2.4	0.32
	332 GHz	$\leq 3\sigma$	-	0.01	-	0.32
N_2H^+	J=1-0	1.59[a]	3.05[b]	0.19	2.5	0.27
N_2D^+	J=2-1	1.20	0.57	0.20	2.3	0.45
	J=3-2	$\leq 3\sigma$	-	0.13	-	-
TMC1-N						
$C^{18}O$	J=1-0	1.89	1.07	0.02	5.4	0.53
		1.17	0.40		6.2	0.32
		0.52	0.14		6.8	0.26
	J=2-1	1.22	0.76	0.07	5.5	0.59
		0.70	0.29		6.1	0.39
$C^{17}O$	J=2-1	0.13[a]	0.077[b]	0.03	5.5	0.55
$H^{13}CO^+$	J=1-0	1.60	1.07	0.04	5.9	0.63
DCO^+	J=2-1[c]	1.84	1.07	0.11	6.0	0.55
	J=3-2	0.77	0.32	0.02	5.9	0.39
NH_2D (ortho)	85 GHz	0.31[a]	0.317[b]	0.02	6.1	0.36
	332 GHz	0.07[a]	0.10[b]	0.02	5.9	-
NH_2D (para)	110 GHz	0.11[a]	0.075[b]	0.01	6.1	0.28
	332 GHz	$\leq 3\sigma$	-	0.03	-	-
N_2H^+	J=1-0	2.23[a]	4.31[b]	0.22	6.0	0.39
N_2D^+	J=2-1	0.48	0.162	0.06	5.9	0.31
	J=3-2	$\leq 3\sigma$	-	0.07	-	-

[a] Strongest hyperfine component.
[b] Sum of all hyperfine components.
[c] Assumed unreliable because of self absorption and not used in reduction, see text.

where ν_{ul} is the frequency of the unsplit transition. The partition function $Q(T_{ex})$ must also be given, and it was obtained by summing up the contributions of the relevant energy levels as listed in the JPL line catalog (Pickett et al. 1998).

It must be pointed out that this method works best when the optical depth in the multiplet is significant and when sufficient information can be extracted from the weaker lines, otherwise an unambiguous determination of both the total optical depth and the derived T_{ex} is impossible. Moreover, if some of the lines in the multiplet overlap (i.e. their position differ by less than their FWHM or thereabouts), Eq. (1) must be corrected to account for mutual shielding. For this reason, we also ran in parallel numerical calculations of the full LTE structure of the given molecule at a given T_{ex}. This alternative approach reproduces the same results only in those cases where the adopted T_{ex} reasonably describes the full structure of the molecule (at least in the low energy levels of importance) and not only the given hyperfine multiplet. In this alternative approach we do attempt to include mutual shielding effects by scaling the intensity of each line in a blend by a factor $\exp(-\tau'/2)$, where τ' is the optical depth of the other lines in the blend. This seems reasonable for the very close overlapping of the two central lines in the NH_2D multiplets, for example.

For the other molecules, since cross sections for collisional excitation are reasonably well known, some insight into the physical conditions of the cloud is possible. This was achieved

Table 3. Column densities

Molecule	Line	LVG[a]				LTE[b]		N (cm^{-2})		
		$n(H_2)$	T_{kin}	T_{ex}	τ	T_{ex}	τ	this work	other	
L134N (30″,18″)										
$C^{18}O$	J=1-0	5.0(4)*	10.0	10.0	0.87	-	-	2.5(15)	1.2(15)[d]	-
	J=2-1			9.8	1.7	-	-			
$C^{17}O$	J=2-1	-	-	-	-	10.0	0.25	4.0(14)	..	-
$H^{13}CO^+$	J=1-0	1.0(5)	10.0	6.7	0.33	-	-	8.5(11)	1.4(12)[d]	-
DCO^+	J=3-2	1.0(5)	10.0	6.1	4.0	-	-	1.0(13)	3.0(12)[h]	-
NH_2D (ortho)	85 GHz	-	-	-	-	6.0	4.9	2.4(14)[i]	-	-
	332 GHz	-	-	-	-		2.1			
NH_2D (para)	110 GHz	-	-	-	-	6.0	1.5	1.7(14)[i]	7.9(13)[j]	-
	332 GHz	-	-	-	-		0.6			
N_2H^+	J=1-0	-	-	-	-	5.0	11.7	1.3(13)	5.7(12)[d]	7.0(12)[f]
N_2D^+	J=2-1	1.0(5)	10.0	5.4	3.4	-	-	4.6(12)	-	-
TMC1-N										
$C^{18}O$[c]	J=1-0	5.0(4)	10.0	10.1	0.46	-	-	2.2(15)	3.4(15)[e]	-
	J=2-1			9.6	0.9	-	-			
$C^{17}O$	J=2-1	-	-	-	-	10.0	$\leq$0.25	$\leq$1.5(14)	..	-
$H^{13}CO^+$	J=1-0	1.0(5)	10.0	7.2	0.81	-	-	3.1(12)	3.2(12)[e]	-
DCO^+	J=3-2	1.0(5)	10.0	5.5	2.5	-	-	5.0(12)	4.3(12)[h]	-
NH_2D (ortho)	85 GHz	-	-	-	-	6.0	0.32	1.5(13)[i]	-	-
	332 GHz	-	-	-	-		0.14			
NH_2D (para)	110 GHz	-	-	-	-	6.0	0.10	1.0(13)[i]	-	-
	332 GHz	-	-	-	-		0.04			
N_2H^+	J=1-0	-	-	-	-	7.0	4.4	1.1(13)	7.0(12)[f]	1.3(13)[g]
N_2D^+	J=2-1	1.0(5)	10.0	4.3	1.2	-	-	9.0(11)	-	-

* The notation 5.0(4) means 5.0×10^4.
[a] LVG model with assumed gas density and temperature. T_{ex} and τ are calculated for the line. See text for adopted collisional cross sections.
[b] LTE model with adopted T_{ex}; τ is calculated for the line. However, when possible both quantities were derived from HFS analysis, see text.
[c] Sum of the v$\simeq$ 5.5 and 6.1 kms^{-1} components, see text.
[d] Swade (1989) (offset 42″,42″).
[e] Pratap et al. (1997)
[f] Benson et al. (1998) (L183(1) = (0″, 40″) off our (0,0) position in L134N, ammonia peak in TMC1).
[g] Hirahara et al. (1995)
[h] Guélin et al. (1982) (80″ beam).
[i] Sum of ortho and para forms. See text for average $N(NH_2D)$ adopted.
[j] Reported for L134N(S) by Saito et al. (2000) at a nearby position (RA(1950) = $15^h51^m31^s.4$, Dec (1950) = -02°43′31″).

applying a non-LTE radiative transfer code in the LVG approximation. The deduced excitation temperatures for the rotational lines of polar molecules are listed in Table 3. As usually found in dense cores, they lie below the assumed kinetic temperature (10 K), i.e., between 5 and 7 K, depending on the line opacity. The uncertainty on the derived column densities, due to both the measurement errors and the uncertainty on the physical conditions, is about a factor of 2.

3.2.1. NH_2D

NH_2D is very abundant in L134N at the selected position, as shown by the large peak intensities (2K and 1K for the strongest hyperfine feature) about ten times larger than the values (0.3 and 0.1 K) towards TMC1-N, despite the fact that these quiescent dark clouds have probably similar physical conditions (total extinction, kinetic temperature and H_2 density). In the case of TMC1-N, the present detection is very close to the upper limit quoted by Olberg et al. (1985) and Saito et al. (2000).

Towards L134N (30″,18″) all lines in the multiplets are well detected, and the central feature shows strong opacity, when comparing with expected LTE optically thin ratios (see last column of Table 1). Thus, we tested the HFS method which can be expected in this case to return reliable determination of the optical depth and T_{ex}, even if it is unclear if and how it accounts for the mutual shielding of the central blend. The derived excitation

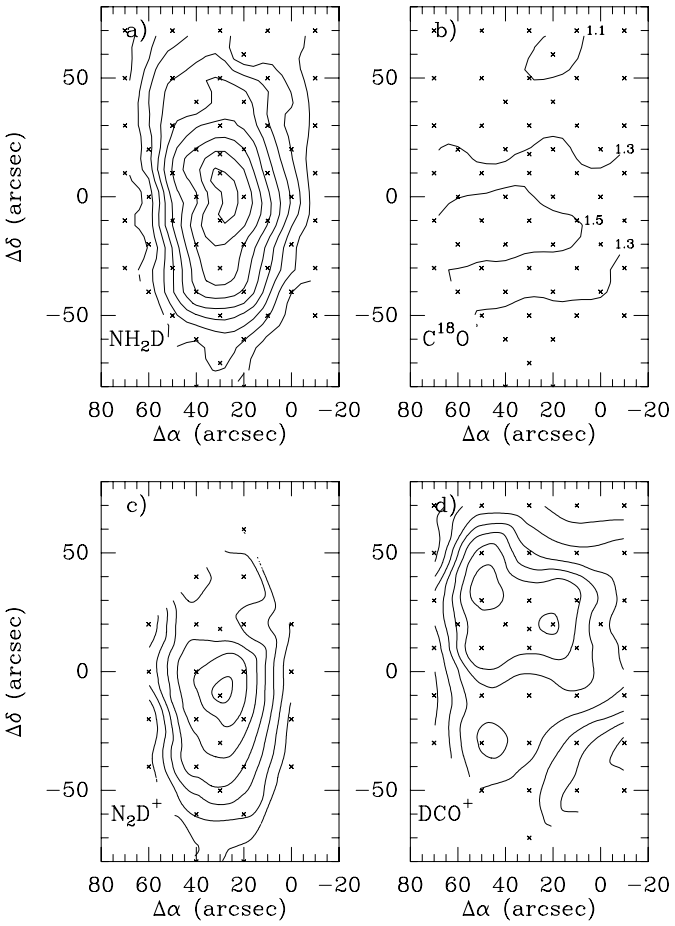

Fig. 2a–d. Maps of the integrated intensity of **a** main hyperfine component of the NH_2D 110GHz transition, **b** $C^{18}O$ (1-0), **c** N_2D^+ (2-1) and **d** DCO^+ (3-2) towards L134N. Contour levels are as follows: **a** from 0.05 Kkms^{-1} to 0.5 Kkms^{-1} by 0.05 Kkms^{-1}, **b** from 1.1 Kkms^{-1} to 1.5 Kkms^{-1}K by 0.2 Kkms^{-1}, **c** from 0.18 Kkms^{-1} to 0.80 Kkms^{-1}K by 0.08 Kkms^{-1} and **d** from 0.1 Kkms^{-1} to 0.6 Kkms^{-1} by 0.06 Kkms^{-1}. For the $C^{18}O$(1-0) map, we display the line intensity integrated from 2 to 3 kms^{-1}, the velocity interval where the NH_2D and DCO^+ emission is detected. The DCO^+(3-2) line is self reversed or flat topped close to the NH_2D peak (see the spectrum shown in Fig. 5).

temperature for the 85 GHz and 110 GHz lines were found to be 5.7 K and 4.6 K, respectively. Since it is unclear why these values should differ for the two multiplets along the same line of sight, we decided to adopt the full LTE approach with T_{ex}=6.0 K for all energy levels below 300K. The observed intensity of the ground state lines at 332 GHz is consistent with T_{ex} = 6K. The results for the column densities are given in Table 3. For the 85 GHz line the column density derived by this method agrees to within 20–30% with the result of the HFS method.

Towards TMC1-N, only the 85 GHz multiplet is sufficiently well resolved for an analysis of hyperfine ratios to be significant. Indeed, the HFS method returns unlikely low values for the excitation temperature ($T_{ex} \simeq$ 3.2 K for both multiplets) which would result in extremely high values of the column density. Thus we adopted T_{ex} = 6.0 K for both lines, to mimic the model discussed above for L134N (30″,18″), and ran a full LTE calculation to obtain the values listed in the table.

Since we adopted LTE models, for lack of data on the collisional excitation of this molecule, the values listed in Table 3 for the column densities of NH_2D, as derived from observations of ortho and para lines, refer to the total for the molecule, not to the ortho and para forms separately (respectively 3/4 and 1/4 of the total at LTE). Thus, ideally, these values should be identical for a given source if LTE is an accurate approximation. The inferred discrepancy is indicative of the uncertainties in the derivation of the column densities from the observed spectra, but the data are reasonably consistent with a standard 3:1 ratio of the ortho to para species. For the chemical modeling of the next section we adopted for the total NH_2D column density the average values: N(NH_2D)=2.0×10^{14} cm^{-2} for L134N and N(NH_2D)=1.3×10^{13} cm^{-2} for TMC1-N.

3.2.2. Other molecules

The CO isotopes, due to their small dipole moment, are practically at LTE with $T_{\rm ex} \simeq T_{\rm kin}$ at densities typical of dense cloud cores such as those studied here. Therefore, from the observed J=2→1/J=1→0 line ratios only a constraint on $T_{\rm kin}$ is obtainable, and we found that the typical value $T_{\rm kin} \simeq$ 10 K is reasonable for both clouds.

A special discussion is necessary regarding the observations of the CO isotopes towards TMC1-N. Previous observations of these isotopes towards TMC1 have shown that there are intervening layers of gas, probably three of them, at different velocities and physical conditions along the line of sight (Pratap et al. 1997). We find clear evidence of these velocity components in both lines observed, see Fig. 5. Disregarding the high velocity component (v $\simeq$ 6.9 kms^{-1}) detected only in the J=1-0 line, and thus probably originating from a very diffuse layer of gas (given the inferred 3σ upper limit on the antenna temperature of the 2-1 line), we have separately modeled the other two velocity components (v $\simeq$ 5.5 kms^{-1} and v $\simeq$ 6.1 kms^{-1}) and found that both were consistent with densities of $few \times 10^4$ cm^{-3}. We adopt n(H_2)=5.0×10^4 cm^{-3}, as a representative value and we add the inferred column densities to determine the value listed in Table 3 for this cloud. Therefore, N($C^{18}O$) adopted here for TMC1-N is probably an upper limit of the real value for the dense molecular gas along the line of sight. For the $C^{17}O$ 2-1 line, the S/N achieved is not sufficient to clearly separate the individual hyperfine lines towards this cloud, with the further splitting due to the multiple velocity components along the line of sight.

Since chemical fractionation effects do not significantly modify the abundance of ^{18}O and ^{17}O containing species, we can directly infer the CO column density by scaling the ones deduced for the minor isotopes by the cosmic fractions [^{16}O]/[^{18}O]=500 and [^{16}O]/[^{17}O]=2925, respectively. Thus, from the $C^{18}O$ column densities listed in Table 3, the CO column density is derived to be 1.3×10^{18} cm^{-2} towards L134N and 1.1×10^{18} cm^{-2} towards TMC1-N. These determinations are within a factor of two of the values quoted by Swade (1989) for

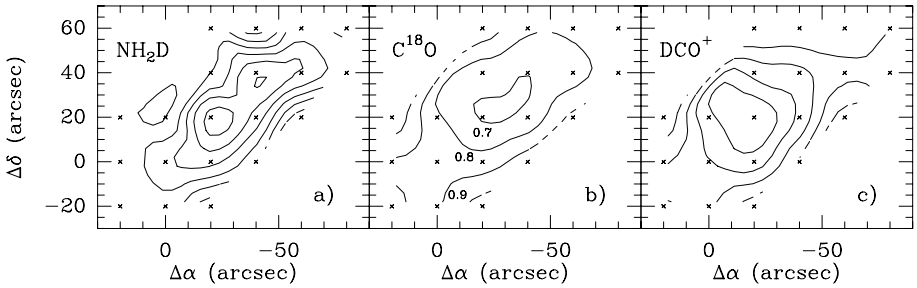

Fig. 3a–c. Maps of the integrated intensity of **a** main hyperfine component of the NH_2D 110GHz transition, **b** $C^{18}O$ (1-0) and **c** DCO^+ (3-2) towards TMC1-N. Contour levels are as follows: **a** 0.01 Kkms^{-1} to 0.06K by 0.01K, **b** 0.6 Kkms^{-1} to 1.1 Kkms^{-1} by 0.1 Kkms^{-1} and **c** 0.12 Kkms^{-1} to 0.4 Kkms^{-1} by 0.04 Kkms^{-1}. Note that for $C^{18}O$ (1-0) (**b**) the integration was limited to the velocity range where the DCO^+ and NH_2D emission is detected: 5.5 to 6.5 kms^{-1}. This map shows a depression at the position of the peak DCO^+ and NH_2D emission.

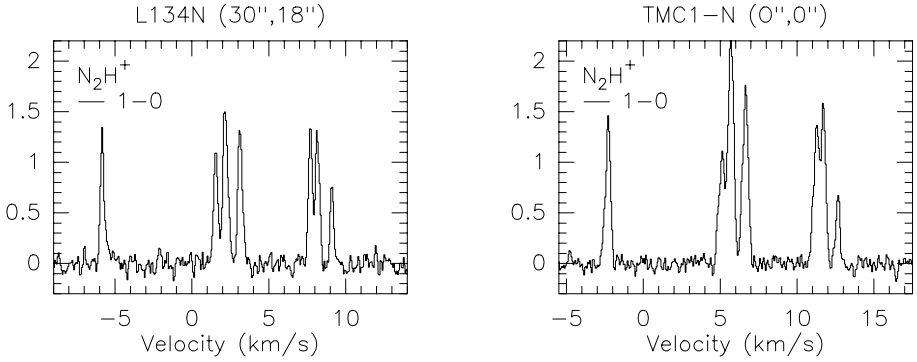

Fig. 4. As in Fig. 1 but for N_2H^+(1-0). Left panel is for L134N (30″,18″), right panel is for TMC1-N (0″,0″). The seven hyperfine components are all individually resolved.

$C^{18}O$ in L134N at various nearby positions. Moreover, our data are consistent with the result we infer for N(CO) (=1.2×10^{18} cm^{-2}) when the $C^{17}O$ column density is considered, instead. In the case of TMC1-N this value of the column density of $C^{18}O$ compares favorably with the result obtained by Pratap et al. (1997) (N($C^{18}O$) $\simeq 3.4 \times 10^{15}$ cm^{-2}). However, this determination is in conflict with the upper limit we give in Table 2 for N($C^{17}O$) (which would convert to a CO column density which is at least a factor of 4 lower). In the following we trust the determination of N(CO) in TMC1-N deduced from the much better detected $C^{18}O$ emission.

Since the cross section for collisional deexcitation of HCO^+ by H_2 (J=0 only) are known (Monteiro 1985; Flower 1999), we adopt these for the $H^{13}CO^+$ and DCO^+ isotopes discussed here and perform a LVG analysis. In order to obtain a good fit to the DCO^+ observations with a realistic value for the gas density, we find that n(H_2)=5×10^4–10^5 cm^{-3} works well for both positions ((30″,18″) in L134N and (0″,0″) in TMC1-N). This result agrees with the value n(H_2) = 6×10^4 cm^{-3} obtained by Pratap et al. (1997) from HC_3N observations at a position only a few arc seconds away in TMC1.

For N_2H^+ (1-0) the seven hyperfine lines are all well separated and reasonably strong. Indeed, the HFS method combined with Eq. 2 reproduces well prior determinations of $T_{\rm ex}$ (see Table 3) by Benson et al. (1998) towards nearby positions in the same dense cores.

Finally, we model the J=2→1 line of N_2D^+ as a single unsplit transition, because the magnitude of the hyperfine splitting of this line, due to both nitrogen nuclei and to deuterium as well, is unknown at present. However, note that some hint of hyperfine splitting is visible in the spectra, see Fig. 5, but the S/N achieved is not high enough to justify an in depth analysis of these effects. We are then able to apply a LVG approach with n(H_2)=10^5 cm^{-3} by adopting the N_2H^+-He collisional deexcitation cross sections, calculated by Green (1975), which were scaled by a factor 1.37 to account for the difference in mass between H_2 and He.

Table 4. Observed molecular fractions

line of sight	$\frac{DCO^+}{HCO^+}$	$\frac{DCO^+}{CO}$	$\frac{NH_2D}{NH_3}$	$\frac{NH_2D}{CO}$	$\frac{N_2D^+}{N_2H^+}$	$\frac{N_2D^+}{CO}$
L134N	0.18	7.7(-6)	0.10	1.5(-4)	0.35	3.5(-6)
TMC1-N	0.02	4.5(-6)	0.02	1.2(-5)	0.08	8.2(-7)

3.2.3. Deuterium fractionation and fractional abundances

The observed deuterium fractionation is obtained from the ratios of the column densities of deuterated species to their major isotopic counterpart which assumes that the cloud is homogeneous. We use the following published NH_3 column densities: 5.4×10^{14} cm^{-2} towards TMC1-N (Pratap et al. 1997) and 2.0×10^{15} cm^{-2} towards L134N (30”,18”) (Swade 1989; Ungerechts et al. 1980). The critical densities related to NH_3 and NH_2D are very different, by at least a factor of 50 coming from the relative Einstein emission transition probabilities. We assume that both molecules are found at the same location as can be plausibly deduced from the maps of NH_3 displayed by Olano

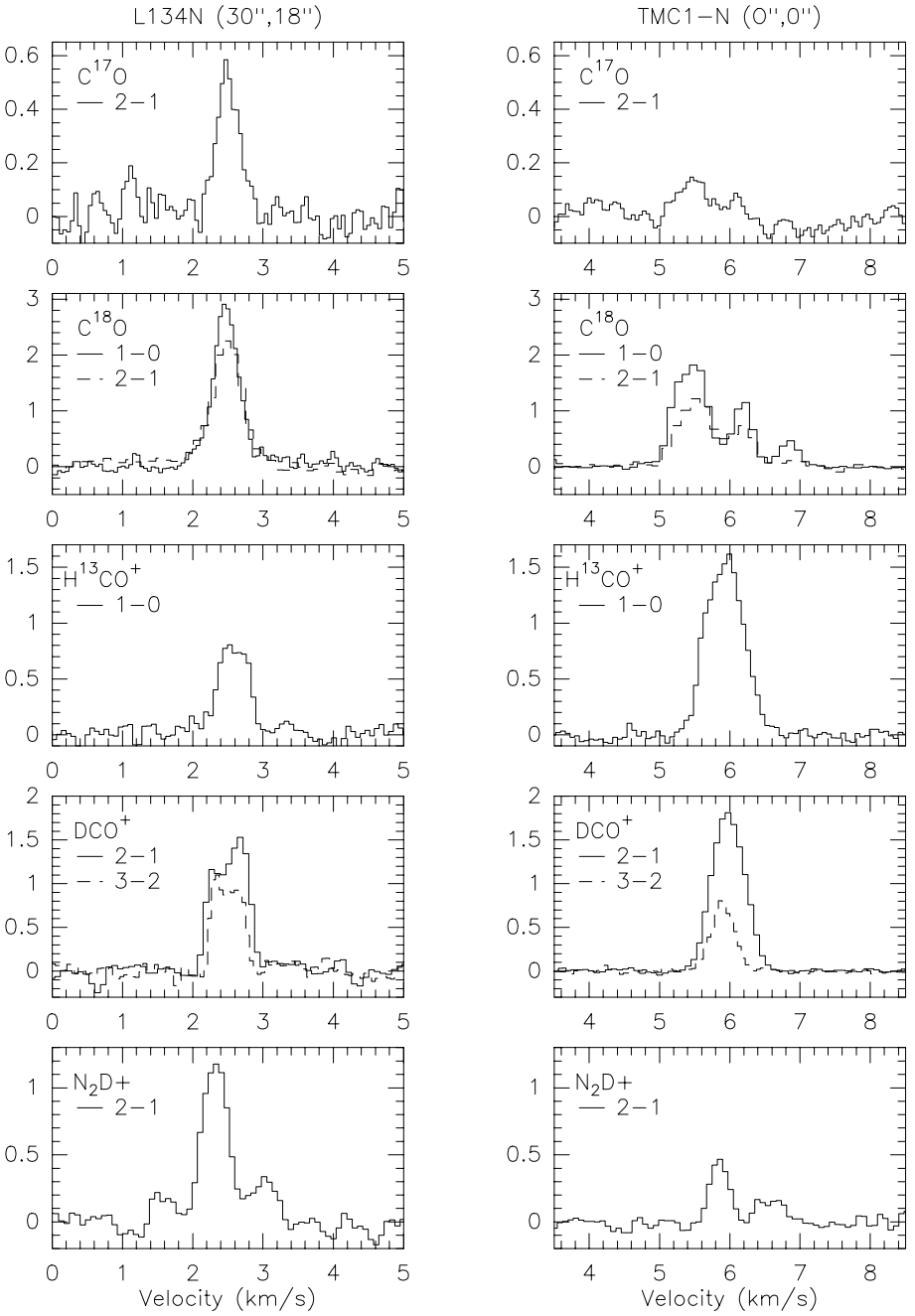

Fig. 5. As in Fig. 1 but for other molecules. Left column is for L134N (30″,18″), right column is for TMC1-N (0″,0″). The velocity range (x-axis) is the same for all spectra, while the antenna temperature range (y-axis) is kept constant for adjacent (left and right) spectra, to aid in the comparison.

et al. (1988) for TMC1 and Ungerechts et al. (1980) for L134N. Table 4 displays the ratios of the observed DCO^+, NH_2D and N_2D^+ column densities to their respective main isotopic counterpart. The HCO^+ column density was inferred from the observed $H^{13}CO^+$ line, scaling the column density by the elemental fraction $[^{12}C]/[^{13}C]\simeq 66$ adopted in this paper (see Table 5, discussed below). We also display the ratios of the presently observed molecular column densities to CO column density. In the next section, we compare these ratios with the predictions from the chemical models since CO is known more accurately than molecular hydrogen. Table 4 shows clearly that the L134N line of sight exhibits an exceptionally large deuterium enhancement in all molecules considered.

4. Dark cloud chemistry

We consider a steady state gas phase chemical network comprising around 2000 reactions linking 200 species, among which all the important ^{13}C and D containing isotopes. We introduce grain surface reactions only for the formation of H_2 and HD. Indeed, Willacy & Millar (1998) have found that the D/H ratio in molecules is relatively independent of the surface processes. The lines of sight under investigation correspond to dark clouds with extinction $A_V > 10$ and photodissociation reactions do not contribute to the chemistry.

The elemental abundances are basic parameters of the model but are not well known in dense clouds. We adopt the values

Table 5. Elemental abundances

Element	Model 1	Model 2
H	1.00	1.00
D	1.00(-5)	1.00(-5)
He	1.00(-1)	1.00(-1)
^{12}C	7.30(-5) [a]	7.30(-6)
^{13}C	1.11(-6) [b]	1.11(-7)
N	1.20(-4)	1.20(-4)
O	1.76(-4) [a]	1.76(-5)
S	2.00(-8) [a]	2.00(-9)
Metals	1.50(-8) [a]	1.50(-8)

[a] Millar et al. (1991)
[b] Langer & Penzias (1993) (see text).

used in the literature (e.g. Millar et al. 1991) which are supposed to reflect a standard interstellar depletion of the elements on grains with the exception of nitrogen atoms, since nitrogen species have been rarely found on grain mantles (Lacy et al. 1998). This set is referred to in the following as model 1, see Table 5. Recent ISOPHOT observations of the L1498 dense core at 100 and 200 μm (Willacy et al. 1998) of the cold dust emission show that the maximum emission at 200 μm lies close to the observed NH_3 peak and coincides with a dip in the $C^{18}O$ emission at the core center. This can be interpreted as a sign of the high depletion of $C^{18}O$. Similar conclusions have been derived by Caselli et al. (1999) from their observations of a large DCO^+/HCO^+ ratio in the starless cloud core L1544. To investigate similar physical conditions we introduce then a second set of elemental abundances, hereafter referred to as model 2, where carbon, oxygen and sulfur are depleted by one order of magnitude compared to model 1, as shown in Table 5.

We compute steady state abundances for a kinetic temperature of 10 K which corresponds to the expected physical conditions of the clouds, for the two mentioned choices of depletions and for a ratio of the proton density n_H to the cosmic ionization rate ζ ranging from 2×10^{20} cm^{-3}s to 10^{22} cm^{-3}s. Since the LVG analysis of the column densities, discussed previously, allows us to deduce molecular hydrogen density, we may infer the cosmic ionization rate when comparing models and observations.

The production of DCO^+ and N_2D^+ from gas phase chemistry has been discussed previously (Guélin et al. 1982). It involves reactions with H_2D^+ and CH_2D^+ which become abundant only at low temperatures. The chemistry of ammonia has been the subject of a variety of papers (Prasad & Huntress 1980a, 1980b; Millar & Freeman 1984; Le Bourlot 1991) and the reaction

$N^+ + H_2 \rightarrow NH^+ + H$

has been often considered as the first step in the synthesis of ammonia. Experiments performed at very low temperatures (Marquette et al. 1985) have shown that this reaction has a small endothermicity of 170K when H_2 is in pure para state J=0 and thus it cannot occur in dark molecular clouds conditions. The corresponding reaction involving HD has a reduced endothermicity of 16.3K so that the reaction may proceed and form ND^+ which reacts with H_2 in a sequence of exothermic reactions up to NH_3D^+, which gives NH_2D via dissociative recombination. The branching ratios obtained in the dissociative recombination reaction of NH_3D^+ are not known and we assume a statistical repartition of the neutral products with the same reaction rate coefficient as NH_4^+. The branching ratios in the dissociative recombination of NH_2^+ and NH_4^+ have been determined experimentally by Vikor et al. (1999). Then, at the very low temperatures found in dark clouds, the gas phase formation route of ammonia becomes (Willacy & Millar 1998):

$N + H_2^+ \rightarrow NH^+ + H$

whose deuterated counterpart is however completely negligible in comparison to the previously mentioned reaction.

An alternative path to the formation of deuterated ammonia has been suggested by Scott et al. (1997) to proceed via the intermediary reaction

$H_3^+ + N \rightarrow NH_2^+ + H$

However, this reaction involves the transfer of two protons and theoretical considerations lead to the result that the corresponding reaction rate coefficient should be small (Herbst et al. 1987). Finally, a new experimental setup showed that the reaction is indeed slow (Scott et al. 1998).

In Figs. 6–8 we show the results for the deuterium fractionation and fractional abundances relative to CO of the three

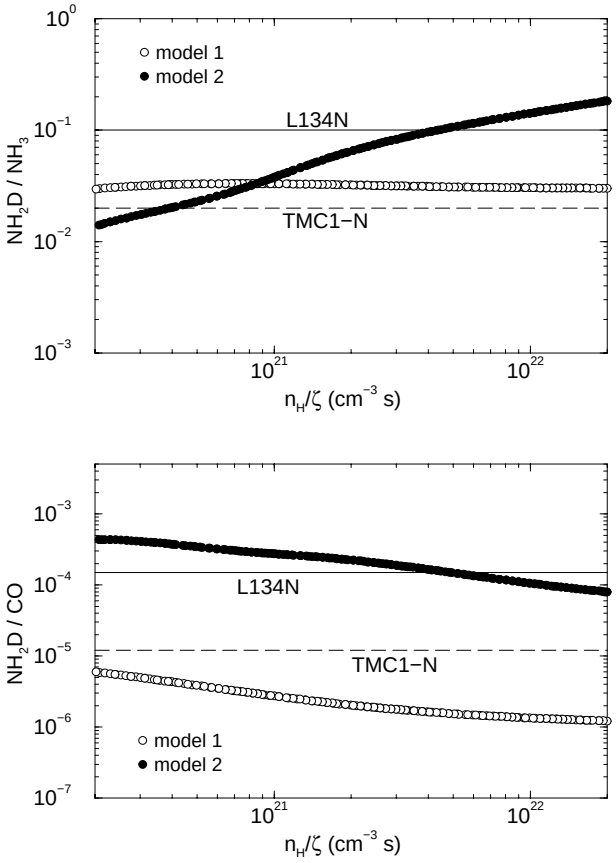

Fig. 6. Molecular fractions calculated as a function of n_H/ζ for a deuterium fractional abundance of 10^{-5}.

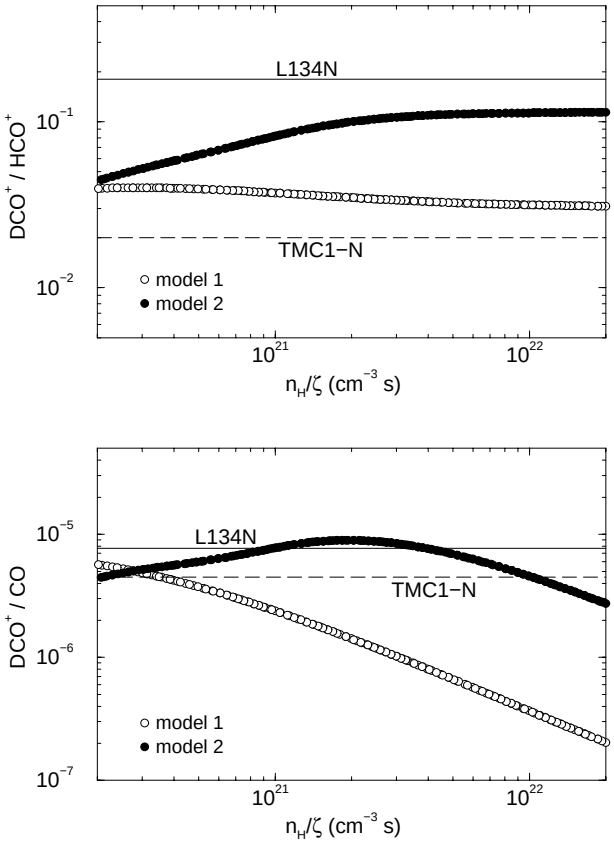

Fig. 7. Molecular fractions calculated as a function of n_H/ζ for a deuterium fractional abundance of 10^{-5}.

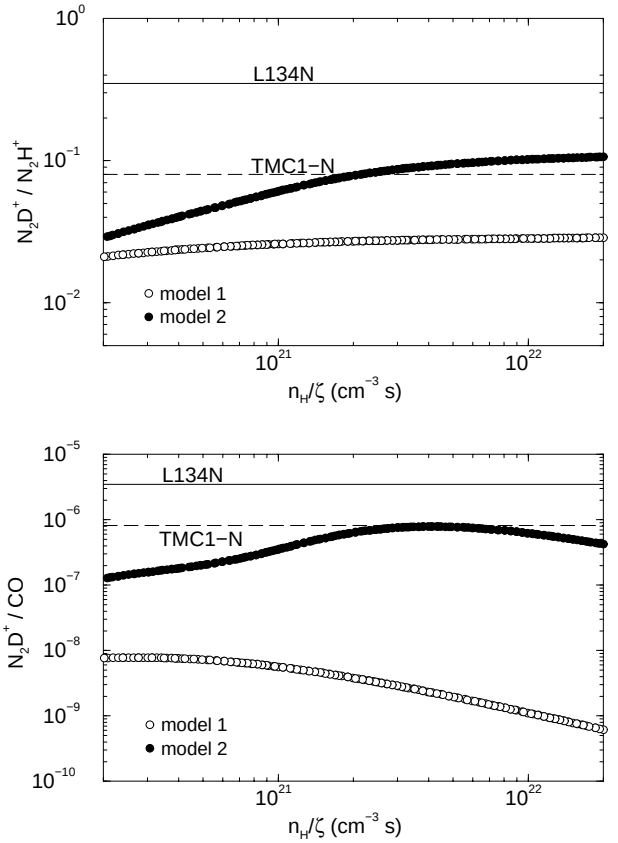

Fig. 8. Molecular fractions calculated as a function of n_H/ζ for a deuterium fractional abundance of 10^{-5}.

molecules under investigation, for the two depletion models. The values inferred from the observations towards L134N and TMC1-N are also shown. Decreasing the gas phase elemental abundances of carbon and oxygen relative to nitrogen and deuterium, while keeping the same [C]/[O] ratio, leads to an increase of the abundance of N_2, N_2D^+ and NH_2D due to the corresponding increase of the H_3^+ and H_2D^+ molecular ions. Indeed, the dominant destruction channel for these ions becomes now electron recombination, rather than reaction with oxygen atoms or CO molecules, even if the fractional ionization is now just $\sim 10^{-8}$. The effect is particularly significant for N_2D^+.

Therefore, a better agreement between chemical models and observed values is obtained when increasing the depletion of carbon and oxygen. Moreover, the models tend to favor large values of the ratio of the proton density n_H to the cosmic ionization rate ζ. Since the H_2 density is found to lie close to 10^5 cm^{-3} from the observations, we find that a cosmic ionization rate ζ of some 10^{-17} s^{-1} is appropriate for the considered clouds.

Several uncertainties remain in the chemical network; amongst them we list as particularly critical the branching ratios of the dissociative recombination of NH_3D^+ and the last step of the exothermic chain reaction $NH_3^+ + H_2$ (and its deuterated version $NH_2D^+ + H_2$). Moreover, the $NH_3^+ + H_2$ ion molecule reaction has a unusually low reaction rate coefficient of about 10^{-12} cm^3 s^{-1} which was measured by Luine & Dunn (1985) in an ion trap and which shows an increase towards very low temperatures. We also assume that the deuterated reaction has the same reaction rate coefficient. Because of these various uncertainties, we consider the agreement towards TMC1-N as reasonable. However, the L134N line of sight shows a particularly large enhancement of deuterated species which could arise from a local enhancement in the deuterium abundance. A [D]/[H] ratio of about 3×10^{-5} would lead to proper agreement with the observations.

5. Conclusion

In this paper we reported about observations of nitrogen containing species towards the ammonia peak in TMC1 and towards a position in L134N which was found to be an ammonia peak. NH_2D was detected for the first time towards TMC1-N. We mapped both clouds in detail around these lines of sight, to elucidate in particular the striking NH_2D emission peak in L134N, stronger than in any other dark cloud, to our knowledge. We applied a pure gas phase chemical model aiming at reproducing the observed column density ratios of deuterated species to their non deuterated counterparts. We found that the observations are compatible with large depletions of carbon and oxygen, as found in other dense cores. The high deuterium fractionation observed towards L134N seems to require a large [D]/[H] ratio of about 3×10^{-5}, which is a factor of 2 above the normal assumed value. The models discussed in the present paper are given at

steady state. It does not seem crucial to involve time dependent effects for the species investigated here, especially for deuterated ammonia. To test further the relation between deuterated molecules and elemental depletion, it would be worthwhile to search for NH_2D and N_2D^+ in other dense cores.

Acknowledgements. We would like to thank L. Coudert for his help checking the molecular properties of NH_2D and the referee for the stimulating comments. ST acknowledges TMR grant ERBFMRXCT97-0132 from the EU. ER and GPdF belong to the UMR8631 of the CNRS, EF and MG to the UMR8540 of the CNRS. The CSO is funded by NSF grant AST96-15025.

References

Benson P.J., Caselli P., Myers P.C., 1998, ApJ 506, 743
Brown R.D., Rice E., 1981, Phil. Trans. R. Soc. London, Ser. A 303, 523
Caselli P., Walmsley C.M., Tafalla M., Dore L., Myers P.C., 1999, ApJ 523, L165
Cohen E.A., Pickett H.M., 1982, J. Mol. Spectrosc. 93, 83
Coudert L.H., 1999, private communication
Cummins S.E., Linke R.A., Thaddeus P., 1986, ApJS 60, 819
Flower D.R., 1999, MNRAS 305, 651
Green S., 1975, ApJ 201, 366
Guélin M., Langer W. D., Wilson R. W., 1982, A&A 107, 107
Herbst E., Defrees D.J., McLean A.D., 1987, ApJ 321, 898
Hirahara Y., Masuda A., Kawaguchi K., et al., 1995, PASJ 47, 845
Irvine W.M., 1998, private communication
Jacq T., Walmsley C.M., Henkel C., et al., 1990, A&A 228, 447
Kuiper T.B.H., Langer W.D., Velusamy T., 1996, ApJ 468, 761
Lacy J.H., Faraji H., Sandford S.A., Allamandola L.J., 1998, ApJ 502, L105
Langer W.D., Penzias A.A., 1993, ApJ 408, 539
Le Bourlot J., 1991, A&A 242, 235
Luine J.A., Dunn G.H., 1985, ApJ 299, L67
Marquette J.B., Rowe B.R., Dupeyrat G., Roueff E., 1985, A&A 147, 115
Millar T.J., Freeman A., 1984, MNRAS 205, 405
Millar T.J., Bennett A., Rawlings J.M.C., Brown P.D., Charnley S.B., 1991, A&AS 87, 585
Monteiro T.S., 1985, MNRAS 214, 419
Myers P.C., Benson P.J., 1983, ApJ 266, 309
Olano C.A., Walmsley C.M., Wilson T.L., 1988, A&A 196, 194
Olberg M., Bester M., Rau G., et al. 1985, A&A 142, L1
Penzias A.A., Wannier P.G., Wilson R.W., Linke R.A., 1977, ApJ 211, 108
Pickett H.M., Poynter R.L., Cohen E.A., et al., 1998, JQSRT 60, 883
Prasad S.S., Huntress W.T. Jr., 1980a, ApJS 43, 1
Prasad S.S., Huntress W.T. Jr., 1980b, ApJ 239, 151
Pratap P., Dickens J.E., Snell R.L., et al., 1997, ApJ 486, 862
Roueff E., Tiné S., Coudert L.H., et al., 2000, A&A Letters, in press
Saito S., Ozeki H., Ohishi M., Yamamoto S., 2000, ApJ, in press
Scott G.B.I., Freeman C.G., McEwan M.J., 1997, MNRAS 290, 636
Scott G.B.I., Fairley D.A., Freeman C.G., McEwan M.J., Anicich V.G., 1998, J. Chem. Phys. 109, 9010
Snell R.L., Wootten H.A., 1977, ApJ 216, L111
Snyder L.E., Hollis J.M., Buhl D., Watson W.D., 1977, ApJ 218, L61
Swade D.A., 1989, ApJ 345, 828
Ungerechts H., Walmsley C.M., Winnewisser G., 1980, A&A 88, 259
Vikor L., Al-Khalili A., Danared H., et al., 1999, A&A, 344, 1027
Willacy K., Millar T.J., 1998, MNRAS 298, 562
Willacy K., Langer W.D., Velusamy T., 1998, ApJ 507, L171
Wootten H.A., Loren R.B., Snell R.L., 1982, ApJ 255, 160